Dyes and Pigments 114 (2015) 93–104

Contents lists available at ScienceDirect

Dyes and Pigments

journal homepage: www.elsevier.com/locate/dyepig

Protonation salt derivative with heavy-atom effect on phthalocyanine for enhanced *in vitro* photodynamic therapy

Xianglan Chen, Yejing Li, Ao Wang, Lin Zhou, Shan Lu, Jiahong Zhou, Yun Lin, Shaohua Wei*

Jiangsu Collaborative Innovation Center of Biomedical Functional Materials, Jiangsu Key Laboratory of Biomedical Materials, School of Chemistry and Materials Science, Analysis and Testing Center, Key Laboratory of Applied Photochemistry, Nanjing Normal University, Nanjing 210023, China

ARTICLE INFO

Article history:
Received 14 August 2014
Received in revised form
28 October 2014
Accepted 3 November 2014
Available online 10 November 2014

Keywords:
Heavy atom heavy
Phthalocyanine
Photodynamic therapy
Water solubility
Anticancer activity
Polyamine

ABSTRACT

In order to improve water-solubility and photodynamic activity of 2(3), 9(10), 16(17), 23(24)-tetra-((amino)methyl)phenoxy)phthalocyaninato-zinc (ZnPc) simultaneously, here, we present the first attempt to introduce heavy atoms (Br and I) to ZnPc though a simple method by synthesizing the hydrobromide and hydriodate protonation salt derivatives of ZnPc. Researches indicated that these protonation salt derivatives of ZnPc can stably disperse in aqueous system for a long time. Furthermore, the internal heavy atom effect from hydriodate in the ZnPc molecules enhances the intersystem crossing (ISC) efficiency of ZnPc during its photo-exciting process. Therefore, the generation of reactive oxygen species (ROSs), especially singlet oxygen ($^1O_2$), is significantly improved, which leads to an improved *in vitro* photodynamic therapy (PDT).

1. Introduction

PDT, a clinical therapeutic modality, has great potential to become an efficient theranostic approach for noninvasive treatment of tumors [1–3]. Its basic principle is as follows: the photosensitizing drug retains in target cells, followed by the excitation by light of a suitable wavelength. Then the light-activated photosensitizers (PSs) transfers the absorbed photon energy to surrounding oxygen molecules, generating cytotoxic ROSs, mainly $^1O_2$ [4,5], which result in the death of tumor cells [6,7].

Pcs-polyamine, a group of hydrophobic PSs, have been intensively investigated due to their potential targeting ability, strong light absorption at PDT windows (600–900 nm) and low intrinsic toxicity; however, the water solubility and ROSs generation ability of Pcs-polyamine is unsatisfactory [8]. Therefore, finding a new method to improve water solubility and photosensitive anti-tumor activity of Pcs-polyamine has attracted great attention in the field of PDT research [9,10]. The classical method was to synthesize the derivatives of Pcs-polyamine. However, this approach involves complicated synthetic steps, which are not general and not always possible [11]. So, finding a simpler way to achieve the goal has attracted much attraction. $^1O_2$ is generally considered to play a main role in PDT process. Therefore, one possible way is to modulate the photo-physical process of Pcs-polyamine by introducing a certain inner molecular interaction to increase the $^1O_2$ generation efficacy.

As shown in Scheme 1, $^1O_2$ is produced through the reaction between the long-lived triplet state of PS ($^3PS_1$*) and surrounding oxygen molecules. Irradiation of a sensitizer with visible light leads at first to the formation of the excited singlet state ($^1PS_1$*) and then by intersystem crossing (ISC) to the excited triplet state ($^3PS_1$*). The energy transfer from $^3PS_1$* to triplet oxygen ($^3O_2$) results in the formation of the highly reactive $^1O_2$, so the quantity of $^1O_2$ is depended on the efficiency of ISC ($^1PS_1$* to $^3PS_1$*). It's well known that the rate of ISC can be increased as a result of enhanced spin-orbit coupling by the presence of heavy atoms [12–14]. So, if we can introduce heavy atoms into the structure of Pcs-polyamine, their photodynamic activity could be greatly increased.

Our previous research indicated that preparing the hydrochloride derivatives of Pcs-polyamine can greatly increase its solubility in aqueous system [8]. Considering this, if we can synthesize hydrobromide and hydriodate derivatives of Pcs-polyamine, both

* Corresponding author. Tel./fax: +86 025 85891761.
E-mail address: shwei@njnu.edu.cn (S. Wei).

http://dx.doi.org/10.1016/j.dyepig.2014.11.002
0143-7208/

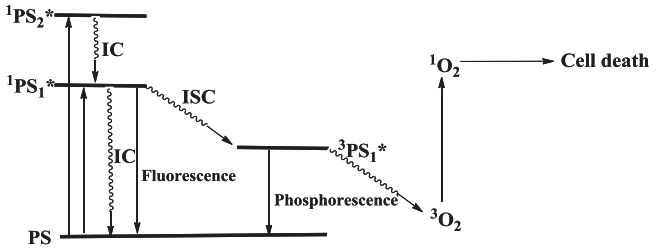

Scheme 1. The diagram depicting the electronic transition states and energy transfer phenomena between the photo-sensitizer molecule and oxygen in photodynamic therapy that ultimately leads to oxidative cell damage.

the water solubility and anti-cancer activity of Pcs-polyamine would be greatly improved. Based on this conception, here, the hydrochloride (**ZnPc1**), hydrobromide (**ZnPc2**) and hydriodate derivatives (**ZnPc3**) of Pcs-polyamine bearing 2(3), 9(10), 16(17), 23(24)-tetra-((amino)methyl)phenoxy)phthalocyaninato-zinc (**ZnPc**) were synthesized and their photodynamic anti-cancer activity were compared. Results indicated that the water solubility of **ZnPc1**, **ZnPc2** and **ZnPc3** was greatly increased. And the introduced heavy atoms can modulate the photo-physical process of ZnPcs, which can improve their $^1O_2$ generation ability and, thereby, the *in vitro* photodynamic efficacy to cancer cells.

2. Experiments

2.1. Materials and characteristics

4-nitrophthalonitrile (**1**) was used after being recrystallized from CH_3OH. 4-(aminomethyl) phenol (**2**), (chloromethanetriyl) tribenzene and other necessary chemicals were obtained from commercial suppliers and used without further purification unless otherwise stated. The 1,8-diazabicyclo[5,4,0]-undec-7-ene (DBU) and the disodium salt of 9,10-anthracenedipropionic acid (ADPA) were from Sigma. 3-[4,5-Dimethylthiazol-2-yl]-2,5-diphenyltetrazolium bromide (MTT) and Hoechst 33342 were from Amosco and used as received. Dulbecco's minimum essential medium (DMEM) and fetal calf serum (FCS) were from Gibico. All organic reagents were of analytical grade and were purified according to reported procedures before use. Thin Layer Chromatography (TLC) was performed on silica gel GF254 plates. Silica gel (300–400 mesh) was used for preparative column chromatography.

Infrared spectra were measured in KBr pelletson on IR-Spectrometer Nicolet Nexus 670. ^1H NMR and ^{13}C NMR spectra were recorded using a Bruker Advance 400 MHz NMR spectrometer. Elemental analyses were taken with Vario MICRO Elementar. The relative content of zinc and chlorine (zinc and bromine, zinc and iodine) of the **ZnPc1** (**ZnPc2** and **ZnPc3**) were obtained using energy dispersive spectrometer (EDS, Noran Vantage, Thermo Norman). UV–Vis spectra were recorded on spectrophotometer Cary 5000, Varian. Fluorescence spectra were recorded on Perkin Elmer LS 50B fluorescence spectrophotometer. The fluorescence lifetimes were determined from time-resolved intensity decay by time-correlated single photon counting (TCSPC) method. A 665 nm LED was used as light source.

2.2. Synthesis of dyes

Compound **3** was prepared from the reaction between compound **1** and compound **2**. Moreover, compound **4** was obtained from the reaction between compound **3** with (chloromethanetriyl) tribenzene that has active –NH groups. K_2CO_3, a base that is often effective in the reaction of a phenol with nitro substituted phthalonitrile at 60 °C, does work well in reaction that generates compound **3**. All spectral data supported the proposed structures of precursor compounds **3**, **4** and **5**.

2.2.1. 4-(4-(aminomethyl)phenoxy)phthalonitrile (3)

4-nitrophthalonitrile (1.41 g, 8.14 mmol), compound 4-(aminomethyl) phenol (1.50 g, 12.18 mmol) and dry K_2CO_3 (2.24 g, 16.21 mmol) were mixed in dry DMF (6 mL) under nitrogen at 60 °C, then CH_2Cl_2 (10 mL) was added as solvent, and they were left to stir for 6 h. During the whole process, the reaction was monitored by TLC using ethyl acetate and a few drops of triethylamine for elution. After cooling to room temperature, the solution was poured into water (80 mL) and a little saturated salt water was added into the above solution. A few minutes later, the mixture was automatically divided into two layers. The upper tangerine solution was the product of synthesis and dried over anhydrous sodium sulfate. In the end, compound **3** was purified by column chromatography with silica gel as column material and methanol/ethyl acetate (2:1) solvent system as elution. Yield: 1.41 g (69.5%). MP. 79 °C. IR (KBr, cm^{-1}): 3364 (NH_2), 3080 (Ar–H), 2840 (CH_2), 2230 (CN), 1590, 1490, 1250, 1070, 710. ^1H NMR (400 MHz, DMSO-d6): δ (ppm) 8.08 (d, 1H, J = 8.8 Hz, Ar), 7.72 (d, 1H, J = 2.8 Hz, Ar), 7.46 (d, 2H, J = 8.8 Hz, Ar), 7.31–7.34 (m, 1H, Ar), 7.13 (d, 2H, J = 8.4Hz, Ar), 3.76 (s, 2H, CH_2), 2.28 (s, 2H, NH_2). ^{13}C NMR (100 MHz, DMSO-d6): δ (ppm) 161.9, 152.4, 142.3, 136.7, 129.6, 122.7, 122, 120.6, 117.1, 116.4, 115.9, 108.3, 45.4. Anal. Calcd. For $C_{15}H_{11}N_3O$: C, 72.28; H, 4.45; N, 16.86; O, 6.42. Found: C, 72.12; H, 4.30; N, 16.78.

2.2.2. 4-(4-((tritylamino)methyl)phenoxy)phthalonitrile (4)

A mixture of anhydrous compound **3** (1.00 g, 4.01 mmol) and finely ground anhydrous K_2CO_3 (1.11 g, 8.02 mmol) in CH_2Cl_2 (40 mL) was stirred under nitrogen at room temperature. Then, (chloromethanetriyl) tribenzene (1.34 g, 4.81 mmol) in CH_2Cl_2 (40 mL) was added dropwise to the solution over a period of 5 h, and the system was stirred for another 2 h after the titration finished. The formed solid material and K_2CO_3 were filtered off and the filtrate was washed with water (3 × 100 mL). The solution was dried over anhydrous sodium sulfate. After filtered, the solvent was evaporated in vacuum; the residue was purified by column chromatography with silica gel as column material and ethyl acetate/petroleum ether (2:1) solvent system as elution. Yield: 1.58 g (80.2%). M.P. 205 °C. IR (KBr, cm^{-1}): 3320 (NH), 3080 (Ar–H), 2840 (CH_2), 2230 (CN), 1590, 1510, 1490, 1250, 710. ^1H NMR (400 MHz, DMSO-d6): δ (ppm) 7.73 (d, 1H, J = 8.8 Hz, Ar), 7.61 (d, 6H, J = 1.2 Hz, Ar), 7.59 (d, 2H, J = 0.8 Hz, Ar), 7.07–7.55 (m, 12H, Ar), 7.056 (d, 2H, J = 2 Hz, Ar), 3.416 (s, 2H, CH_2), 1.96 (s, 1H, NH). ^{13}C NMR (100 MHz, DMSO-d6): δ (ppm) 162.0, 152.2, 145.8, 139.3, 135.4, 130.1, 128.6, 128.0, 127.9, 127.3, 126.5, 121.4, 121.3, 120.6, 117.6, 115.5, 115.0, 108.7, 71.0, 47.3. Anal. Calcd. For $C_{34}H_{25}N_3O$: C, 83.07; H, 5.13; N, 8.55; O, 3.25. Found: C, 82.02; H, 5.08; N, 8; O, 3.18.

2.2.3. 2(3), 9(10), 16(17), 23(24)-tetra-((tritylamino)methyl) phenoxy) phthalocyaninato-zinc (5)

The same procedure was used for the synthesis of the compound **5** in literature. Compound **5** was synthesized with addition of substituted phthalonitrile compound **4** (700 mg, 1.42 mmol) and stoichiometric amounts of related anhydrous metal salts $Zn(CH_3COO)_2$ (163.28 mg, 0.89 mmol) to the reaction media at reflux temperature in n-pentanol (6 mL) and by the catalyst of DBU (200 μL) for 24 h. After precipitating the crude products in CH_3OH (80 mL), the deep blue solid product was washed with H_2O and CH_3OH till the filtrate was colorless. The green crud product was

purified by passing through a sillica gel column with dichloromethane/methyl alcohol (1:5). Yield: 1.576 g (80.0%). M.P. >200 °C. IR (KBr, cm^{-1}): 3490, 3425, 3130, 1620, 1400, 1230, 1040, 710, 486. ^1H NMR (400 MHz, DMSO-d6): δ (ppm) 7.61–7.59 (br, 16H, Pc-H), 7.56 (s, 4H, Pc-H), 7.50 (s, 4H, Pc-H), 7.39–7.28 (m, 60H, Pc-H), 7.08 (s, 4H, Pc-H), 3.36 (s, 8H, CH_2). ^{13}C NMR (100 MHz, DMSO-d6): δ (ppm) 146.1, 136.4, 129.6, 128.7, 128.0, 127.8, 127.6, 126.4, 120.3, 119.4, 119.2, 117.0, 102.7, 98.9, 77.4, 51.6, 49.5, 47.5, 45.8, 43.1, 31.9, 29.7, 9.8, 6.8. Anal. Calcd. For $C_{136}H_{100}N_{12}O_4$: C, 80.40; H, 4.96; N, 8.27. Found: C, 80.20; H, 4.78, N, 8.28.

2.2.4. 2(3), 9(10), 16(17), 23(24)-tetra-((amino)methyl)phenoxy) phthalocyaninato -zinc(ZnPc)

Under the condition of ice-water bath, compound **5** (500 mg, 0.25 mol) and excess trifluoroacetic acid (TFA) (0.5 mL) were dissolved in CH_2Cl_2 (10 mL) and stirred for 1 h. Then, the reaction mixture was heated to room temperature and left to stir for another 2 h. The crude product was collected by filtration and washed successively with CH_2Cl_2. Thereafter, the green solid was dissolved in H_2O and precipitated by adjusting PH to 9–10. The residue product collected by filtration was washed successively with H_2O and CH_3OH. The product was vacuum-dried at 50 °C for 12 h to afford the final. M.P. >200 °C. IR (KBr, cm^{-1}): 3410, 3240, 2840 (CH_2), 2230 (CN), 1630, 1420, 1120, 1005, 620. ^1H NMR (400 MHz, DMSO-d6): δ (ppm) 12.7 (s, 8H, NH_2), 8.98–8.96 (br, 4H, Pc-H), 8.55 (s, 4H, Pc-H), 8.37 (s, 4H, Pc-H), 7.78–7.66 (br, 8H, Pc-H), 7.54–7.45 (br, 8H, Pc-H), 3.36 (s, 8H, CH_2). ^{13}C NMR (100 MHz, $CDCl_3$): δ (ppm) 159.4, 159.07, 158.7, 157.9, 157.7, 135.0, 131.7, 130.3, 129.2, 127.1, 124.6, 121.5, 119.8, 119.4, 117.5, 114.6, 115.0, 108.2, 103.4, 100.1, 45.9. Anal. Calcd. For $C_{60}H_{44}N_{12}O_4$: C, 67.83; H, 4.17; N, 15.82. Found: C, 67.44; H, 4.22; N, 15.70.

2.2.5. Hydrochloride, hydrobromide and hydriodate derivative of 2(3), 9(10), 16(17), 23(24)-tetra-((amino)methyl)phenoxy) phthalocyaninato-zinc (ZnPc1, ZnPc2 and ZnPc3)

ZnPc1 (**ZnPc2**, **ZnPc3**) was suspended in 5 mL redistilled water in a reaction bulb and warmed to reflux. Excess 5% HCl (HBr, HI) aqueous was added into the solution drop-wise until **ZnPc1** (**ZnPc2**, **ZnPc3**) was totally dissolved under 40 °C. After adding solution into the acetone, the crude precipitation was collected by filtration, then thoroughly washed by dichloromethane and dried in vacuum. The title product **ZnPc1** (**ZnPc2**, **ZnPc3**) was obtained as dark blue solid. Yield: 0.23 g (93.8%). The relative content of elemental chlorine (bromine and iodine) in **ZnPc1** (**ZnPc2**, **ZnPc3**) was analyzed through EDS. Quantitative analysis shows that the mean atomic ratio of Cl/Zn (Br/Zn and I/Zn) of **ZnPc1** (**ZnPc2**, **ZnPc3)** respectively was 0.188 (0.186 and 0.186). Compared with the standard value 0.125, the results confirmed our desired outcomes that one **ZnPc1** (**ZnPc2**, **ZnPc3**) molecule contains eight HCl (HBr and HI) in its structure. Since the elemental analysis, FT-IR, ^1H NMR spectroscopy, electronic spectroscopy and mass spectra of three ZnPcs are analogous to those of compound ZnPc, they are not described in detail here.

2.3. Photodegradation studies

Photostability studies of ZnPcs used in this work were carried out in H_2O by monitoring the decrease in the Q-band absorption before and after irradiation with 665 nm LED using UV–Vis spectrophotometer.

2.4. $^1O_2$ generation detection

$^1O_2$ is one of the most active traits among the reactive oxygen and holds a prominent role in various biological and chemical processes [15,16]. $^1O_2$ was generated by photoexcitation of the ZnPcs molecules in their soret band with laser pulses at $k = 355$ nm followed by the energy transfer between the triplet state of ZnPcs and the ground state of the solvated O_2 molecules. $^1O_2$ generation was determined by the ADPA bleaching method. ZnPcs (5×10^{-6} M) and ADPA (5.5×10^{-6} M) were mixed and irradiated. The reaction was monitored spectrophotometrically by measuring the decrease in optical density every 1 min at an absorbance maximum of 378 nm of ADPA. All samples were air equilibrated.

2.5. Cellular uptake of ZnPc1, ZnPc2 and ZnPc3 in HeLa cells

HeLa cells were incubated under the same experimental conditions with **ZnPc1**, **ZnPc2** and **ZnPc3** (the concentration: 1.5 μM) for respectively 2, 4, 6 and 24 h in the dark. After respectively 2, 4, 6 and 24 h incubation, the drug concentration remaining in the medium was detected and calculated. All cellular uptake amounts were calculated according to the standard curves.

2.6. Intracellular ROSs detection by DCFH-DA

In order to evaluate the ability of the ZnPcs to generate ROS *in vitro*, the probe DCFH-DA was used as a fluorescent probe [17,18]. The non-fluorescent DCFH-DA can be oxidized to the fluorescent DCF in the presence of ROSs. At first, cells (with about 60% confluence) in a 6-well plate suspension in the medium were combined with **ZnPc1**, **ZnPc2** and **ZnPc3**, and incubated in incubator (37 °C, 5% CO_2) for 24 h. Then, the plates were washed with sterile PBS, and the DCFH-DA was added into the wells. After incubation for 0.5 h, cells were washed with PBS and illuminated for about 15 min.

2.7. Cell morphology

For routine maintenance, HeLa cells were cultured in suspension in DMEM medium supplemented with 10% FCS and incubated at 37 °C in humidified air with 5% CO_2. Cell growth inhibition was evaluated using a standard colorimetric MTT assay [19]. Before treatment with ZnPcs, the cells were seeded in 96-well plates and incubated overnight. The density of cells in the medium was about 10,000 cells per well. After treatment with ZnPcs overnight and being irradiated by light, cells were washed with PBS three times and the cell morphology changes were observed under a fluorescence microscope.

2.8. Hoechst 33342 staining

Chromatin condensation was detected by nuclear staining with Hoechst 33342 [20]. After treatment with ZnPcs overnight and being irradiated by light, cells were washed with PBS three times and treated with 25 μg mL^{-1} Hoechst 33342 at 37 °C with 5% CO_2 in the dark for 30 min. Nuclear morphology change was observed under a fluorescence microscope.

2.9. Darktoxicity

In the cytotoxicity test, the same concentrations of ZnPcs were suspended in DMEM and were ultrasonicated for 30 s to prevent agglomeration. To determine the darktoxicity, HeLa cells were seeded into 96 well plates at a density of 5×10^5 cells/cm^2 and incubated for 24 h in growth medium to allow for attachment. Cell cytotoxicity was assessed by using the classical MTT colorimetric assay [21,22].

2.10. In vitro anti-cancer activity studies

For photo-induced anti-cancer experiments, HeLa cells were incubated as described above, and 24 h later, the old medium was replaced by fresh medium (without FCS) with **ZnPc1**, **ZnPc2** or **ZnPc3**, separately. Following 24 h incubation, the culture medium was replaced by FCS-free medium and rinsed for three times by PBS to remove adhered drugs. The cells were immediately exposed to light (10 W) and after 24 h incubation, cells viability was measured as described above [23].

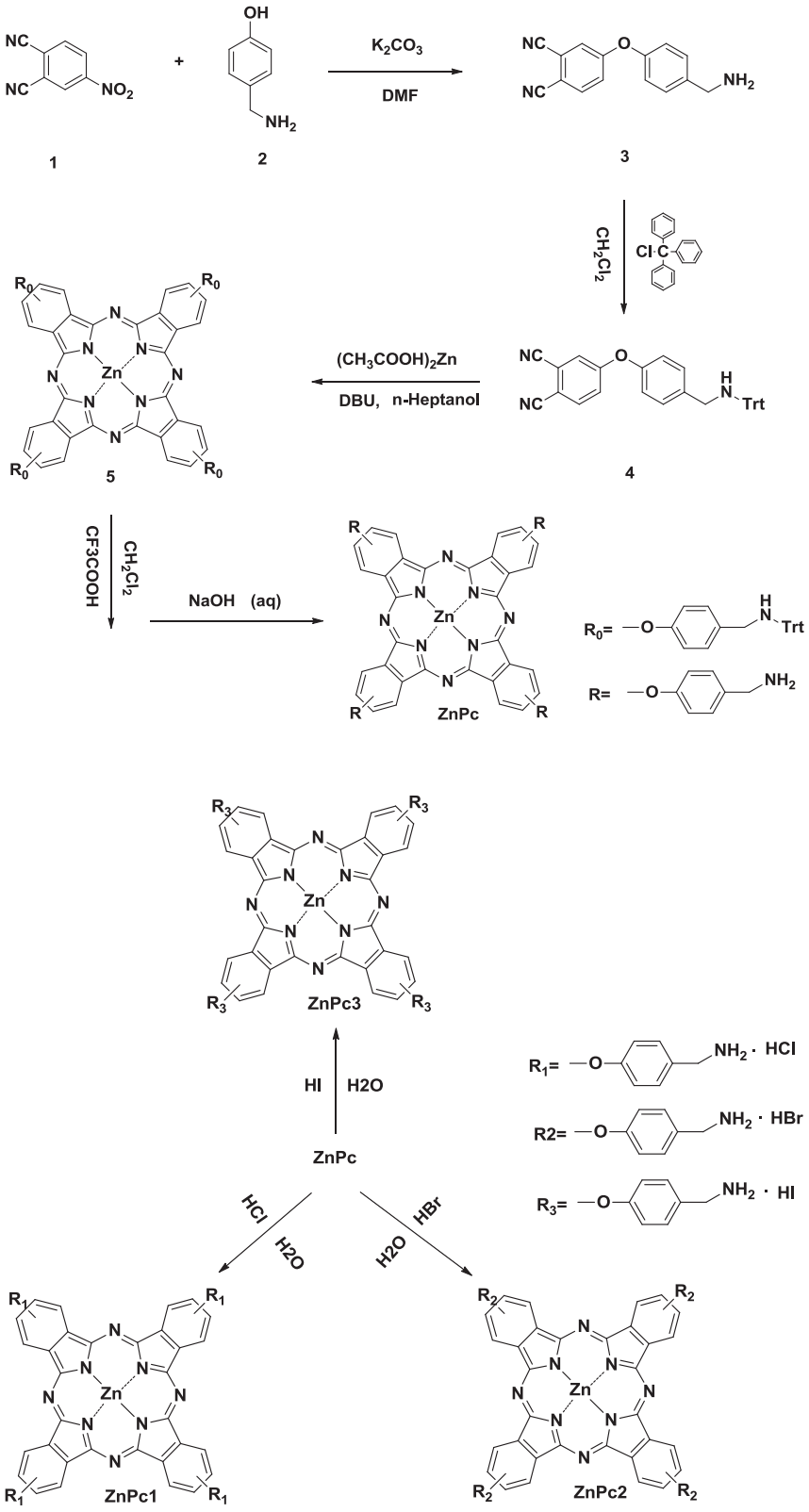

Scheme 2. The synthetic route of the novel phthalonitrile (**3** and **4**) and phthalocyanine compounds (**5**, **ZnPc**, **ZnPc1**, **ZnPc2** and **ZnPc3**).

2.11. Statistical analysis

The assay was conducted with three replicates for each treatment. Data were expressed as mean ± SD of the indicated number of experiments. Statistical differences in dark cytotoxicity and phototoxicity potential assay were determined using *Student's* test. $P < 0.05$ was considered to be statistically significant.

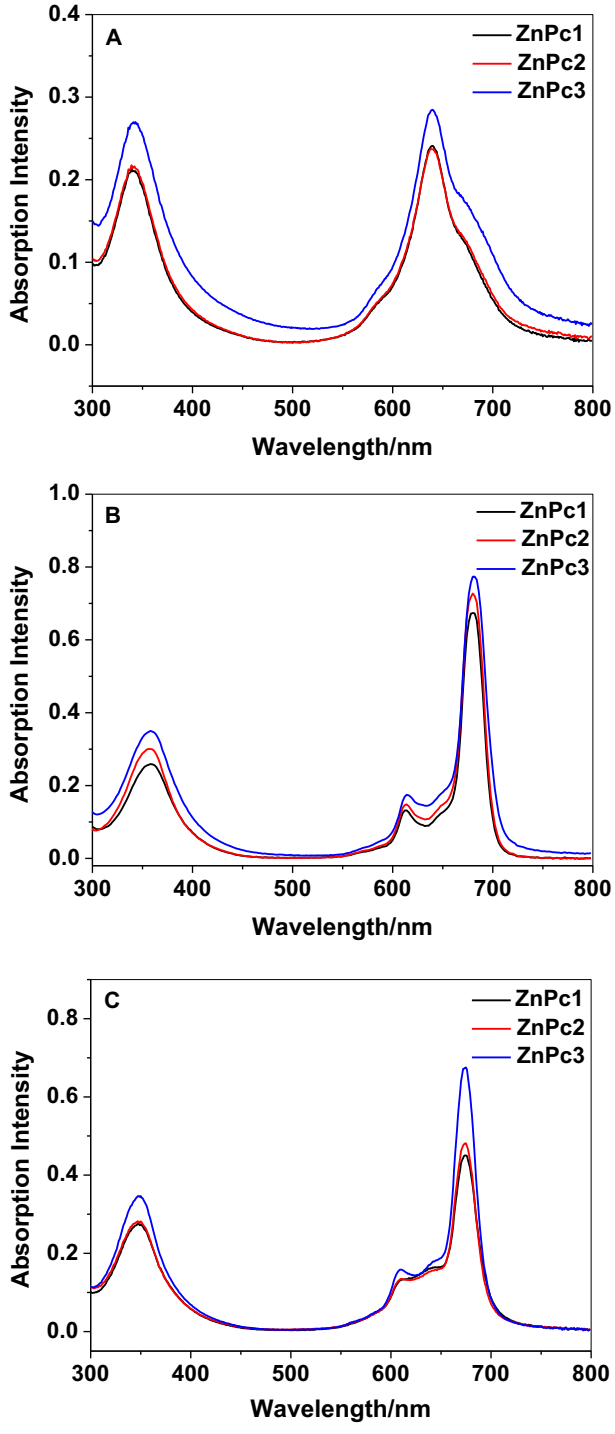

Fig. 1. Absorption spectra of the **ZnPc1**, **ZnPc2** and **ZnPc3** in H_2O (A), DMSO (B) and CH_3OH (C). (Concentration = 5×10^{-6} M).

3. Results and discussion

3.1. Synthesis

The synthetic route employed to access three dyes (**ZnPc1**, **ZnPc2** and **ZnPc3**) is shown in Scheme 2. The dyes were prepared from ZnPc, which was synthesized according to a published procedure [8,9]. **ZnPc1**, **ZnPc2** and **ZnPc3** of Pcs-polyamine bearing ZnPc were synthesized and their photodynamic anti-cancer activity were compared though the present paper. Notably, the water solubility of **ZnPc1**, **ZnPc2** and **ZnPc3** was greatly increased. And the introduced heavy atom can modulate the photophysical process of ZnPcs, which can improve their $^1O_2$ generation ability and, thereby, the *in vitro* photodynamic efficacy to cancer cells.

3.2. Aggregation studies

Molar extinction coefficient (ε) is depended on the physical and chemical properties of PSs and subsequently affected the $^1O_2$ production efficiency and *in vitro* anti-cancer activity. Therefore, ε values of **ZnPc1**, **ZnPc2** and **ZnPc3** in different polar solvents, such as H_2O, DMSO and CH_3OH (solvents polar: H_2O > DMSO > CH_3OH), were studied by UV–Vis spectra. The typical UV–Vis spectra of the ZnPcs usually exhibited characteristic monomer absorption band ~680 nm with aggregate absorption band at 630–640 nm [24,25]. The three ZnPcs all formed aggregates in H_2O, while showed monomeric behaviors in CH_3OH and DMSO. As shown in Fig. 1, the absorbance intensity of **ZnPc1**, **ZnPc2** and **ZnPc3** in different polar solvents were different, which indicated that they had different ε values in these solutions. As shown in Table 1, these values suggested that **ZnPc3** had the sharpest intensity in H_2O, CH_3OH and DMSO in Q bands which due to the electronic structure of the heavy atom ZnPc rings are perturbed resulting in alternation of the ground and excited state electronic structures. Comparing studies indicated that with the change of the structure, the ε also changed thus enhances the absorption intensity, which implies its strong photodynamic activity.

3.3. Fluorescence spectra and properties

To avoid being quenched by water, the fluorescence spectra and time-resolved fluorescence measurements of the ZnPcs were carried out in CH_3OH. As shown in Scheme 1, the electrons in the ground state (PS) are excited to the vibrational levels of excited state ($^1PS_1^*$) during the electronic excitation process. Then the electrons in the vibrational levels of excited state fall to the major singlet excited state via vibrational relaxation. Finally, the electrons in the major singlet excited state can return to any one of the vibrational levels of ground state (PS), with the fluorescence emission [12,26]. In addition, the heavy-atom effect of **ZnPc2** and **ZnPc3** results in higher spin-orbit coupling parameter and faster intersystem crossing (ISC). Thus the density of electrons accumulating in the triple state increases. Since many electrons hop to the triplet state, the emitting fluorescence of the minor and major

Table 1
Lambert–Beer's law generated related constant as shown in Table 1.

Compound	ε_{ZnPc1} (H_2O)	ε_{ZnPc2} (DMSO)	ε_{ZnPc3} (CH_3OH)
ZnPc1	0.0482	0.134	0.090
ZnPc2	0.0473	0.145	0.096
ZnPc3	0.0570	0.155	0.135

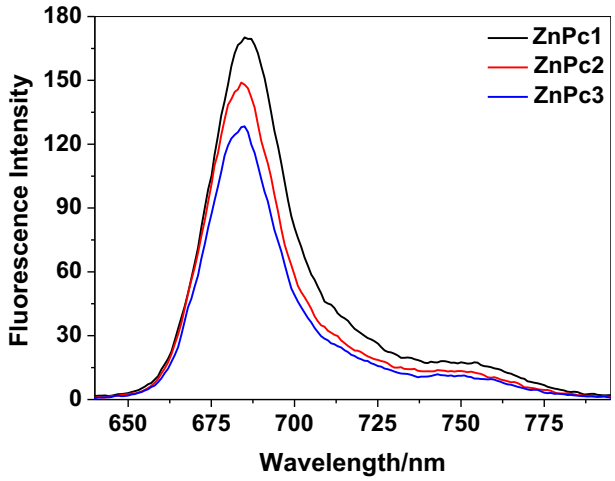

Fig. 2. Fluorescence spectra of the **ZnPc1**, **ZnPc2** and **ZnPc3** in CH_3OH. Concentration = 5×10^{-6} M; Excitation wavelengths: 610 nm.

singlet excited state (600–750 nm) drop dramatically. So, as shown in Fig. 2, it was clear to see that the fluorescence intensity significantly reduced in **ZnPc2** and **ZnPc3** compared to that in **ZnPc1**.

3.4. Time-resolved fluorescence spectra

The fluorescence lifetimes of ZnPcs have been proved to be important parameters for practical applications of fluorescence and ROS generation process [27]. So, to further confirm the heavy atom effect in **ZnPc2** and **ZnPc3**, time-resolved fluorescence experiments were conducted. Time-resolved fluorescence measurements of ZnPcs were made by using 625 nm diode laser excitation and the decay curves of ZnPcs were shown in Fig. 3. The fluorescence lifetimes of the ZnPcs were obtained by the method of time-correlated single-photon counting (TCSPC). The average lifetimes of **ZnPc1**, **ZnPc2** and **ZnPc3** were 3.3 ns ($\chi^2 = 0.96$), 3.0 ns ($\chi^2 = 0.96$), and 2.8 ns ($\chi^2 = 0.90$), respectively. The decrease in fluorescence lifetimes of **ZnPc2** and **ZnPc3** compared with that of **ZnPc1** can be caused by the presence of heavy atom effect which can enhance spin-orbit coupling and, correspondingly, there is an increase in the probability of the ISC. In this case, with an increase in population of the triplet level, an increase in $^1O_2$ sensitization may also occur, which could further support that the heavy-atom effect did take place in the ZnPcs.

3.5. Photodegradation studies

Photostability is very important for PSs in PDT process. The ideal PSs should have high photostability to avoid the PSs molecule destruction during irradiation process [28,29]. Photodegradation was characterized by the decrease in the intensity of the Q band in the absorption spectra on exposure to light of ZnPcs. The spectral changes during irradiation was given in Fig. 4 and the Q band absorbance of the ZnPcs barely decreased during light irradiation, which indicated that **ZnPc1**, **ZnPc2**, and **ZnPc3** all had great photostability. As a result, this pentad dye showed appropriate stability for photo-induced anti-cancer applications.

3.6. $^1O_2$ generation detection

$^1O_2$ is one of the most active traits among the ROSs and holds a prominent role in the processes of PDT [30,31]. Generation of $^1O_2$ was detected by the chemical trapping method, using the ADPA as a $^1O_2$ sensor. To avoid chain reactions induced by ADPA in the presence of $^1O_2$, the concentration of ADPA was lowered to 5×10^{-5} M. ADPA is bleached by $^1O_2$ to its corresponding endoperoxide. We have monitored $^1O_2$ generation by detecting the characteristic peak of ADPA locating at 378 nm under irradiation by 665 nm LED and the rate of $^1O_2$ was calculated by the following Eq [15].:

$$\ln([ADPA]_t/[ADPA]_0) = -kt$$

where $[ADPA]_t$ and $[ADPA]_0$ are the concentrations of ADPA after and prior to irradiation, respectively. Values of k are the rate constant for the quenching of excited PSs by triplet oxygen to produce $^1O_2$ and t is the time of irradiation. Fig. 5 showed the decays of the signal intensity at 378 nm for **ZnPc1**, **ZnPc2**, and **ZnPc3** in 5 min, under irradiation by 665 nm LED (interval time: 1 min). All of the ZnPcs could induce photo-oxidation of ADPA (Fig. 5A–C) and the exact reaction rate constant (k) followed the order $k_{\mathbf{ZnPc3}}$ (0.10452, $R_{\mathbf{ZnPc3}} = 0.999$) > $k_{\mathbf{ZnPc2}}$ (0.08432, $R_{\mathbf{ZnPc2}} = 0.998$) > $k_{\mathbf{ZnPc1}}$ (0.07205, $R_{\mathbf{ZnPc1}} = 0.991$) (Fig. 5D), which indicated that the $^1O_2$ generation ability of **ZnPc3** and **ZnPc2** were superior to that of **ZnPc1**. Along with the enhanced $^1O_2$ generation efficiency, the phototoxic efficacy could also be enhanced. To check this, we have performed a comparative study of the *in vitro* photo-induced anticancer activity of **ZnPc1**, **ZnPc2**, and **ZnPc3**.

3.7. Darktoxicity

Since undesired side effects on normal tissues are one of the major obstacles in clinical PDT, low darktoxicity is an important criterion for assessing the efficacy of a PS. In order to evaluate the darktoxicity of the ZnPcs, HeLa cells were exposed to increasing concentrations of ZnPcs for 24 h and their viabilities were determined using the MTT assay. The darktoxicity results showed that ZnPcs were unharmful to cells in the dark even under a relatively high concentration (1.5 μM, Fig. 6), showing low darktoxicity of all samples at the drug concentration below 1.5 μM.

3.8. Cellular uptake of ZnPc1, ZnPc2 and ZnPc3 in HeLa cells

For the purpose of killing cancer cells, nontoxic light sensitive ZnPcs need to sneak into the cancer cells first [19]. The uptake of the ZnPcs into HeLa cells *in vitro* was studied under different incubation time with ZnPcs of same concentration (1.5 μM). As shown in Table 2, **ZnPc1**, **ZnPc2** or **ZnPc3** all could be effectively taken up by cancer cells and the cell uptaken percents gradually increased with the increasing incubation time. When the incubation time was up to 24 h, there was no apparent difference among the three ZnPcs in the uptake into HeLa cells. So the light-induced anticancer activity studies were carried out after 24 h incubation of these drugs.

3.9. Cell morphological studies

Light induced cytotoxic effects of **ZnPc1**, **ZnPc2** and **ZnPc3** were shown in Fig. 7. 480 nm light irradiation of the drug-free cells did not show any significant changes in cell morphology (Fig. 7A). On the contrary, drastic changes in the morphology were detected in the **ZnPc1** (Fig. 7B), **ZnPc2** (Fig. 7C), or **ZnPc3** (Fig. 7D) and 15 min irradiation treated HeLa cells. These cells shrank and fragmented. These changes were associated with cell death and apparently induced by the ROSs generated by PSs.

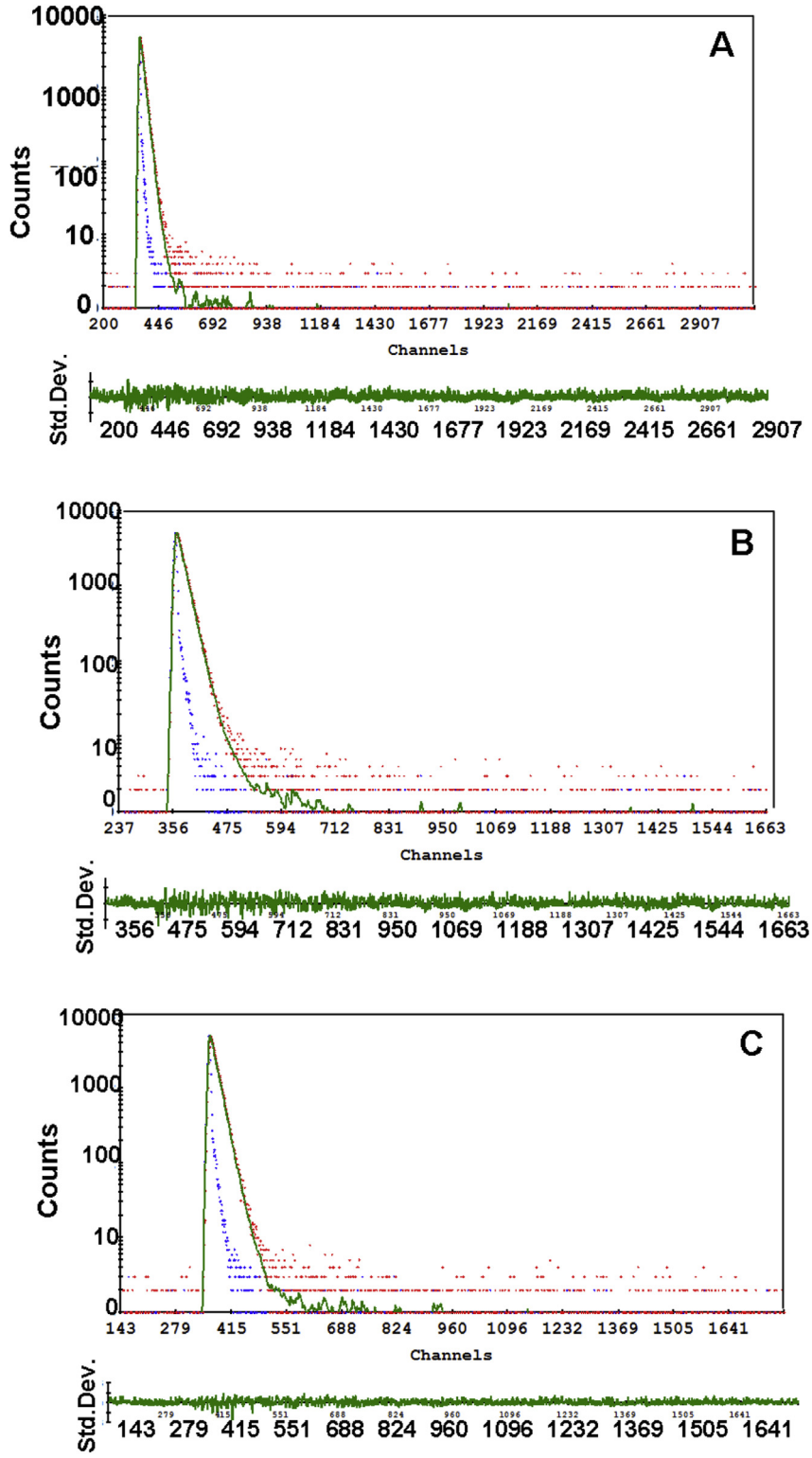

Fig. 3. Time-resolved fluorescence decays for **ZnPc1** (A), **ZnPc2** (B) and **ZnPc3** (C). (Concentration = 10^{-5} M).

3.10. Hoechst 33342 staining

In order to study the photo-damage effect of the ZnPcs on DNA, HeLa cells were stained with Hoechst 33342. Hoechst 33342, a cell-penetrate nuclear probe that emits blue fluorescence when bound to DNA, was used to assess DNA changes in nuclear [32]. The results showed that there was no significant change in cell nuclear morphology when they were irradiated by 665 nm LED for 15 min. The dim fluorescence of chromatin occupied the majority of the HeLa cells (Fig. 8A). In contrast, after irradiation, **ZnPc1** (Fig. 8B), **ZnPc2** (Fig. 8C) and **ZnPc3** (Fig. 8D) treated HeLa cells showed obvious changes in DNA characteristics, such as shrinkage, chromatin condensation, and fragmentation under the same conditions.

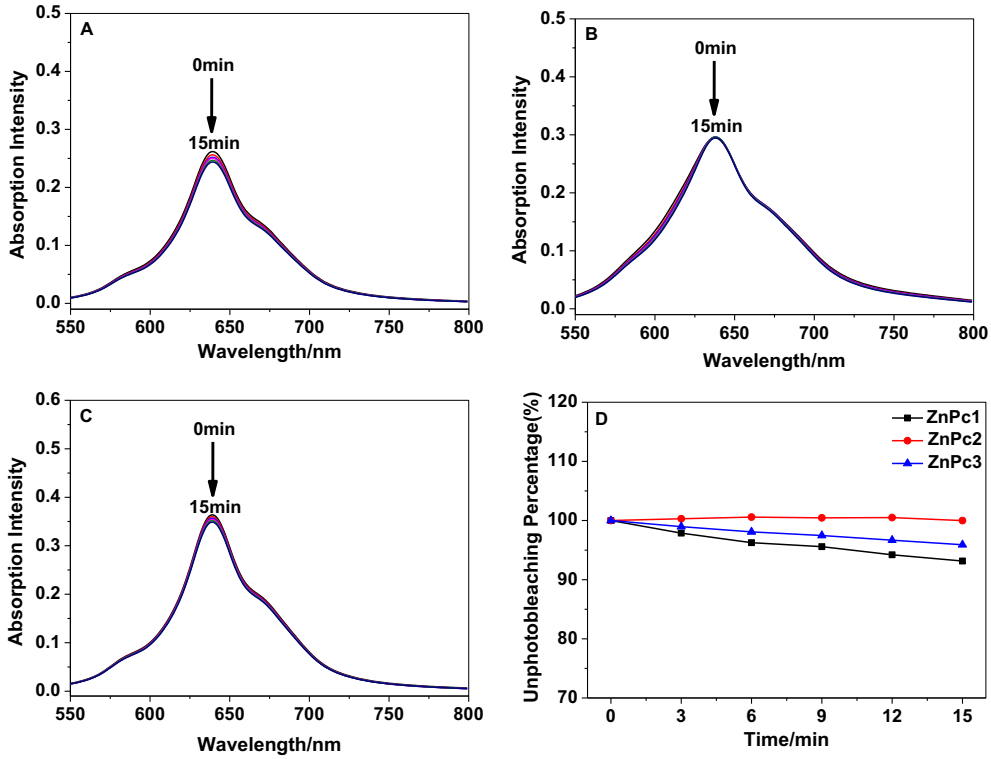

Fig. 4. Absorption spectra changes of **ZnPc1** (A), **ZnPc2** (B) and **ZnPc3** (C) irradiated with 665 nm LED in H_2O; Photo-bleaching properties of the three ZnPcs with 665 nm LED in H_2O (D); (Concentration $= 5 \times 10^{-6}$ M).

3.11. $^1O_2$ production of ZnPc1, ZnPc2 and ZnPc3 in HeLa cells

To further confirm the ROSs generation capability of ZnPcs, DCFH-DA was used as ROSs trapping reagent to obtain the ROSs generation ability through the changes in fluorescence intensity before and after irradiation. As seen in Fig. 9, obvious DCF fluorescence was detected from the **ZnPc1**, **ZnPc2** and **ZnPc3** treated HeLa cells after irradiation by 665 nm LED, which indicated that they could effectively generate ROSs inside the cells. Compared with **ZnPc1**, the ROSs generation ability of **ZnPc3** obviously

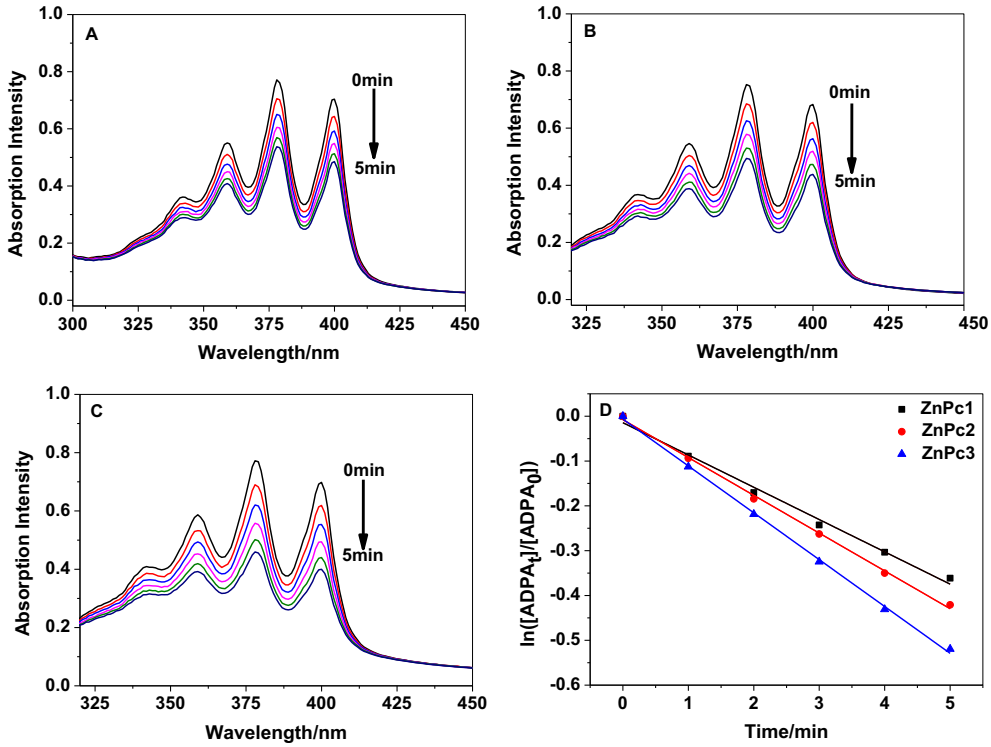

Fig. 5. Absorption spectra of ADPA in **ZnPc1**, **ZnPc2** and **ZnPc3** were irradiated for 0, 1, 2, 3, 4, and 5 min in H_2O.

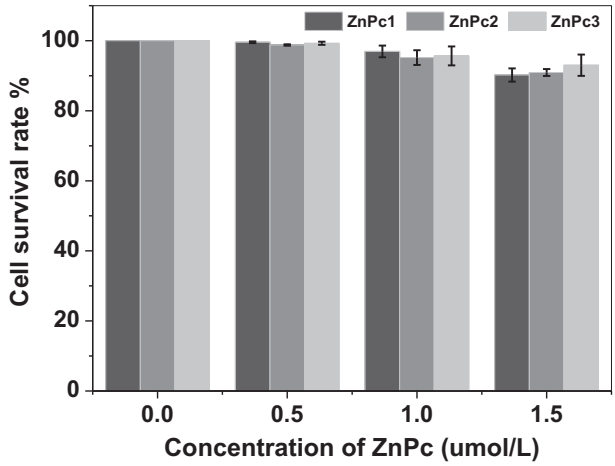

Fig. 6. Dark cell-viability assays with different drug doses of **ZnPc1**, **ZnPc2** and **ZnPc3** to HeLa cells; (Control: cells were treated without ZnPcs).

Table 2
Cellular uptake percent of **ZnPc1**, **ZnPc2** and **ZnPc3** with prolonged incubation time.

Compound	Cellular uptake percent			
	2 h	4 h	6 h	24 h
ZnPc1	32.3%	47.7%	55.3%	75.7%
ZnPc2	29.5%	41.0%	47.6%	73.6%
ZnPc3	24.9%	35.6%	41.5%	72.6%

increased while that of **ZnPc2** obviously decreased, which was different with $^1O_2$ detection results using ADPA as a probe.

3.12. Photo-induced anti-cancer activity

PDT is superior in targeting damages to tumor tissue because of it's the low darktoxicity and high phototoxicity. So, selectively irradiating tumor tissue can active the PS assembling at tumors, lead to a localized phototoxicity effect, thus leave the healthy cells unaffected. All drugs were essentially non-cytotoxic in the absence of light (Fig. 6), but displayed different degrees of phototoxicity. The phototoxicity study, represented in (Fig. 10), showed the percentage of cell survival after treatment of 1.5 μM ZnPcs and 15 min illumination by 665 nm LED lamp. After irradiation, **ZnPc1**, **ZnPc2** and **ZnPc3** all can induce tumor cell death and the anti-cancer activity of **ZnPc3** was obviously higher than that of **ZnPc1** and **ZnPc2** because of the heavy atom effect.

3.13. $^1O_2$ production of ZnPc1, ZnPc2 and ZnPc3 in HeLa cell lysates

Interestingly, previous results indicated that **ZnPc2** had high $^1O_2$ generation ability using ADPA as probe, however, it had low *in vitro* ROSs generation ability and anti-cancer activity in cancer cells compared to **ZnPc1** and **ZnPc3**, which was possibly because of the affect of physiological or bimolecular environment inside the cancer cells [33,34].

To approve this hypothesis, the $^1O_2$ generation abilities of **ZnPc1**, **ZnPc2** and **ZnPc3** were compared in cell lysates. The result was shown in Fig. 11. Compared to the results in pure water, the order of singlet oxygen generation ability of the ZnPcs changed to **ZnPc3** ($k_{\mathbf{ZnPc3}} = 0.096$, $R_{\mathbf{ZnPc3}} = 0.981$) > **ZnPc1** ($k_{\mathbf{ZnPc1}} = 0.049$,

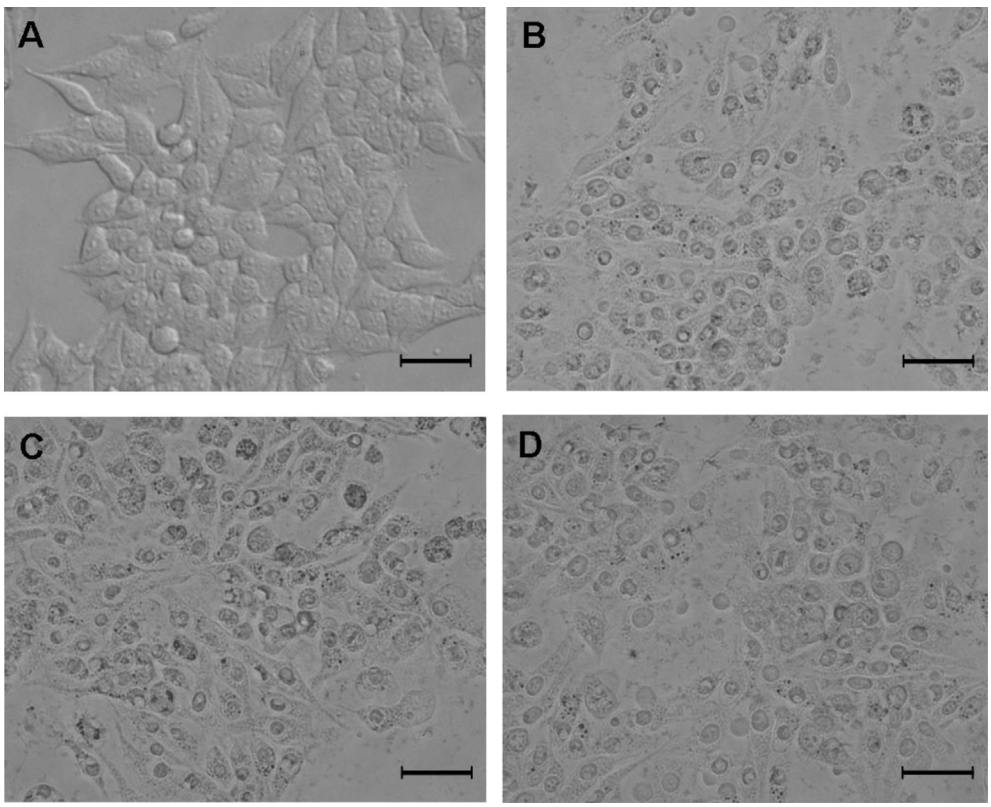

Fig. 7. Microscope images of common HeLa cells (A) and cells treated with **ZnPc1** (B), **ZnPc2** (C) and **ZnPc3** (D) and irradiated for 15 min with 665 nm LED. 40 microscope objective. Bar = 100 μm. (Concentration = 1.5×10^{-6} M).

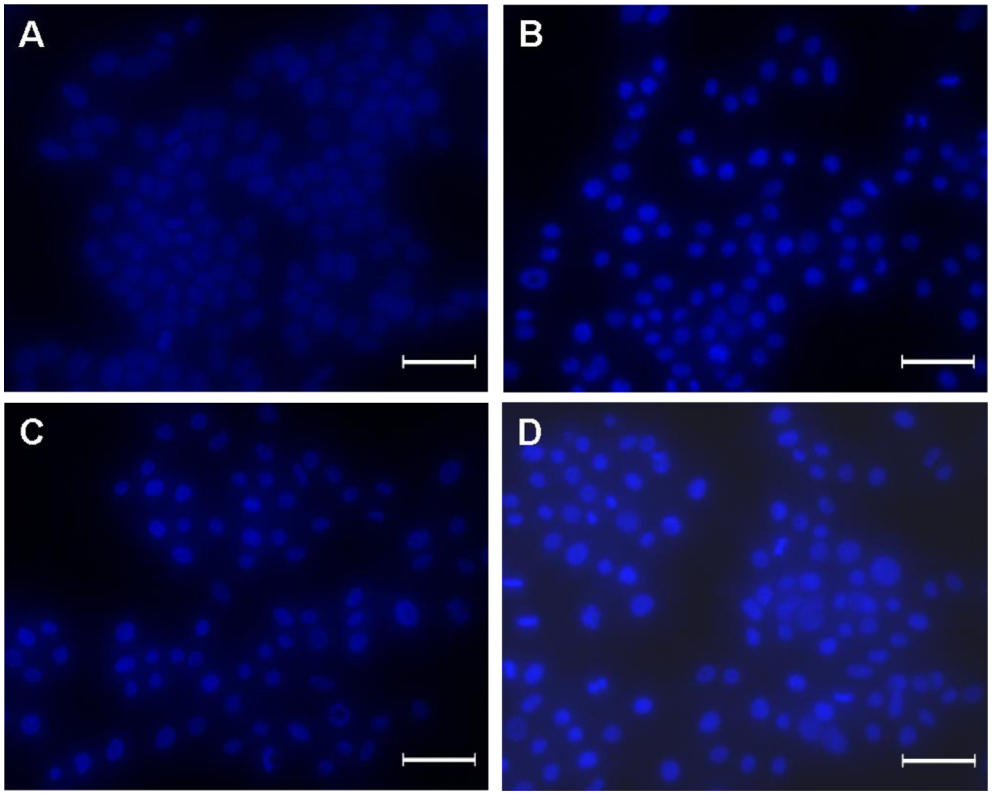

Fig. 8. Fluorescence micrographs of HeLa cells stained with Hoechst 33342. (A) Normal cells; (B) Cells treated with **ZnPc1** and 15 min of irradiation; (C) Cells treated with **ZnPc2** and 15 min of irradiation; (D) Cells treated with **ZnPc3** and 15 min of irradiation. Bar = 100 μm. (Concentration = 1.5×10^{-6} M).

$R_{\mathbf{ZnPc1}} = 0.989$) > **ZnPc2** ($k_{\mathbf{ZnPc2}} = 0.018$, $R_{\mathbf{ZnPc2}} = 0.991$) in cell lysates. The $^1O_2$ generation rates of **ZnPc2** was much lower than **ZnPc1** and **ZnPc3**, which was in agreement with the previously studies of ROSs generation and *in vitro* anti-cancer activity.

4. Conclusion

To improve water-solubility and photodynamic activity of Pcs-polyamine for PDT simultaneously, here, we presented the first attempt to introduce heavy atoms into ZnPc rings by a simple method of synthesizing the protonation salt formulation of Pcs-polyamine. Researches indicated that hydriodate derivatives could disperse in aqueous system and be stable for a long time. Furthermore, the internal heavy atom effect on the ZnPc molecules significantly enhanced the efficiency of $^1O_2$ generation, and thereby, the *in vitro* PDT efficacy because the internal heavy atom effect significantly enhanced the ISC efficiency in the photo-exciting process. Moreover, all of the results demonstrated that above method was a simple but effective way to improve water-solubility and PDT efficiency of Pcs-polyamine simultaneously.

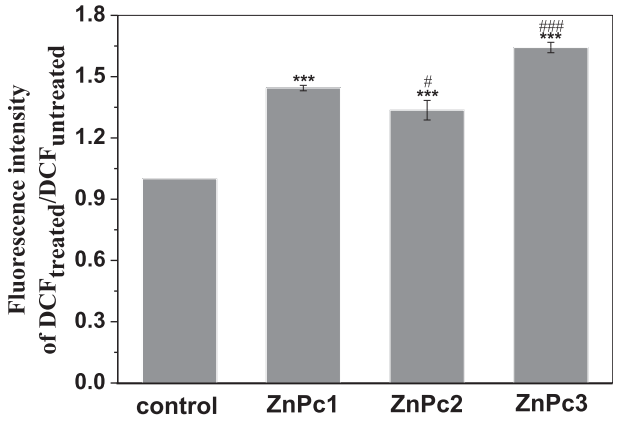

Fig. 9. ROSs generation efficiency of **ZnPc1**, **ZnPc2** and **ZnPc3** inside the HeLa cells. ($^{***}P < 0.001$ vs. Control; Control: cells were exposed to light without ZnPcs, $^{\#}P < 0.05$, $^{\#\#\#}P < 0.001$ vs. ZnPc1).

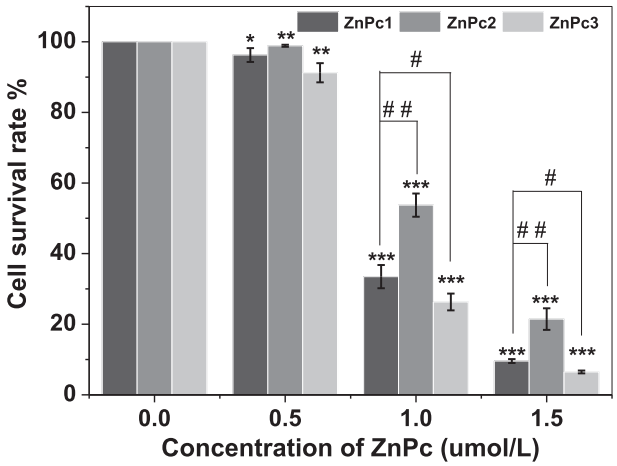

Fig. 10. Comparative *in vitro* light-induced toxicity of **ZnPc1**, **ZnPc2** and **ZnPc3** under the same experimental condition (1.5 μM, irradiation by 480 nm LED) ($^{*}P < 0.05$, $^{**}P < 0.01$ $^{***}P < 0.001$, photo-induced toxicity of ZnPcs versus photo-induced toxicity of control; Control: cells were exposed to light without ZnPcs, $^{\#}P < 0.05$, $^{\#\#}P < 0.01$, photo-induced toxicity of **ZnPc3** or **ZnPc2** versus photo-induced toxicity of **ZnPc1**).

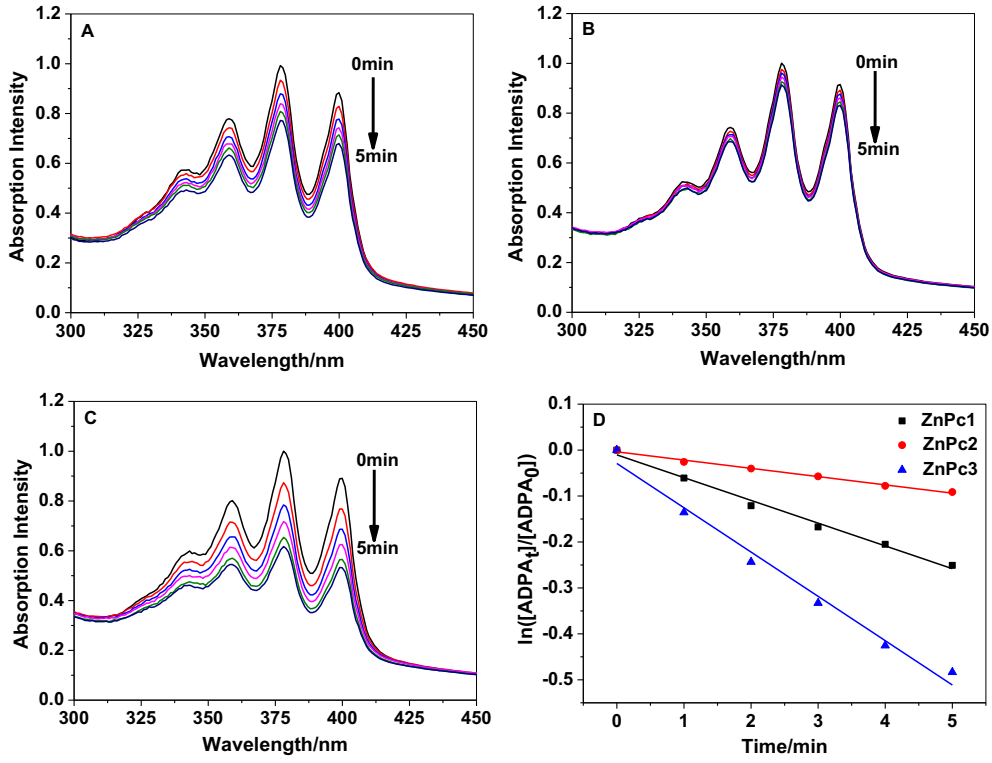

Fig. 11. Time-dependent bleaching of ADPA caused by $^1O_2$ generated by **ZnPc1** (A), **ZnPc2** (B) and **ZnPc3** (C) upon 378 nm photo-irradiation was monitored as a function of time in cell lysates. (D) The best fit of $^1O_2$ generation to the experimental points of **ZnPc1**, **ZnPc2**, and **ZnPc3**.

Acknowledgments

This research was supported by the National Natural Science Foundation of China (21201102), the Scientific Research Foundation of Nanjing Normal University (No. 2011103XG0249), the Natural Science Foundation of Jiangsu Higher Education Institutions of China (No. 13KJA150003, 12KJB150015), the Priority Academic Program Development of Jiangsu Higher Education Institutions (PAPD) and the Foundation of Jiangsu Collaborative Innovation Center of Biomedical Functional Materials.

References

[1] Celli JP, Spring BQ, Rizvi I, Evans CL, Samkoe KS, Verma S, et al. Imaging and photodynamic therapy: mechanisms, monitoring, and optimization. Chem Rev 2010;110:2795–838.
[2] Agostinis P, Berg K, Cengel KA, Foster TH, Girotti AW, Gollnick SO, et al. Photodynamic therapy of cancer: an update. CA – Cancer J Clin 2011;61:250–81.
[3] Yang YT, Chen CT, Tsai TM. Absorption and fluorescence spectral properties of hematoporphyrin in liposomes, micelles, and nanoparticles. Dye Pigment 2013;96:763–9.
[4] Almeida RD, Manadas BJ, Carvaho AP, Duarte CB. Intracellular signaling mechanisms in photodynamic therapy. Biochim Biophys Acta 2004;1704:59–86.
[5] Hirakawa K, Nishimura Y, Arai T, Okazaki S. Singlet Oxygen generating activity of an electron donor connecting porphyrin photosensitizer can be controlled by DNA. J Phys Chem B 2013;117:13490–6.
[6] Kastle M, Grimm S, Nagel R, Breusing N, Grune T. Combination of PDT and inhibitor treatment affects melanoma cells and spares keratinocytes. Free Radic Biol Med 2011;50:305–12.
[7] Charron G, Stuchinskaya T, Edwards DR, Russell DA, Nann T. Insights into the mechanism of quantum dot-sensitized singlet oxygen production for photodynamic therapy. J Phys Chem C 2012;116:9334–42.
[8] Wang A, Ma YJ, Zhou L, Lu S, Lin Y, Zhou JH, et al. Comparison of two strategies for conferring water solubility to a zinc phthalocyanine substituted with 1,2-diethylamino. Dye Pigment 2013;99:348–56.
[9] Sol V, Lamarche F, Enache M, Garcia G, Granet R, Guilloton M, et al. Polyamine conjugates of meso-tritolylporphyrin and protoporphyrin IX: potential agents for photodynamic therapy of cancers. Bioorg Med Chem 2006;14:1364–77.
[10] Durmus M, Ahsen V. Water-soluble cationic gallium (III) and indium (III) phthalocyanines for photodynamic therapy. J Inorg Biochem 2010;104:297–309.
[11] Obata M, Hirohara S, Tanaka R, Kinoshita I, Ohkubo K, Fukuzumi S, et al. In vitro heavy-atom effect of palladium(II) and platinum(II) complexes of pyrrolidine-fused chlorin in photodynamic therapy. J Med Chem 2009;52:2747–53.
[12] Kim S, Ohulchanskyy TY, Bharali D, Chen YH, Pandey RK, Prasad PN. Organically modified silica nanoparticles with intraparticle heavy-atom effect on the encapsulated photosensitizer for enhanced efficacy of photodynamic therapy. J Phys Chem C 2009;113:12641–4.
[13] Zhou L, Ge XF, Liu JH, Zhou JH, Wei SH, Li FY, et al. Internal heavy atom effect of Au(III) and Pt(IV) on hypocrellin A for enhanced in vitro photodynamic therapy of cancer. Bioorg Med Chem Lett 2013;13:5317–24.
[14] Zhou L, Wei SH, Ge XF, Zhou JH, Yu BY, Shen J. External heavy-atomic construction of photosensitizer nanoparticles for enhanced in vitro photodynamic therapy of cancer. J Phys Chem B 2012;116:12744–9.
[15] Tada H, Shiho O, Kuroshima K, Koyama M, Tsukamoto K. An improved colorimetric assay for interleukin 2. J Immunol Methods 1986;93:157–65.
[16] Hussain A, Gadadhar S, Goswami TK, Karande AA, Chakravarty AR. Photoactivated DNA cleavage and anticancer activity of pyrenyl-terpyridine lanthanide complexes. Eur J Med Chem 2012;50:319–31.
[17] Yang YW, Hsu PYJ. The effect of poly(D,L-lactide-co-glycolide) microparticles with polyelectrolyte self-assembled multilayer surfaces on the cross-presentation of exogenous antigens. Biomaterials 2008;29:2516–9.
[18] Spagnuolo G, Anto VD, Cosentino C, Schmalz G, Schweikl H, Rengo S. Effect of N-acetyl-L-cysteine on ROS production and cell death caused by HEMA in human primary gingival fibroblasts. Biomaterials 2006;27:1803–9.
[19] Roy I, Ohulchanskyy TY, Pudavar HE, Bergey EJ, Oseroff AR, Morgan J, et al. Ceramic-based nanoparticles entrapping water-insoluble photosensitizing anticancer drugs: a novel drug-carrier system for photodynamic therapy. J Am Chem Soc 2003;125:7860–5.
[20] Conte C, Ungaro F, Maglio G, Tirino P, Siracusano G, Sciortino MT, et al. Biodegradable core-shell nanoassemblies for the delivery of docetaxel and Zn(II)-phthalocyanine inspired by combination therapy for cancer. J Control Release 2013;167:40–52.
[21] Deng H, Liu X, Xie J, Yin R, Huang N, Gu Y, et al. Quantitative and site-directed chemical modification of hypocrellins toward direct drug delivery and effective photodynamic activity. J Med Chem 2012;55:1910–9.
[22] Lokesh KS, Adriaens A. Synthesis and characterization of tetra-substituted palladium phthalocyanine complexes. Dyes Pigm 2013;96:269–77.

[23] Zhou L, Liu JH, Zhang J, Wei SH, Feng YY, Zhou JH, et al. A new sol-gel silica nanovehicle preparation for photodynamic therapy in vitro. Int J Pharm 2010;386:131–6.
[24] Leznoff CC, Lever ABP. Phthalocyanines: properties and applications. 4th ed. New York: VCH; 1996.
[25] Durmus M, Nyokong T. Synthesis and solvent effects on the electronic absorption and fluorescence spectral properties of substituted zinc phthalocyanines. Polyhedron 2007;26:2767–76.
[26] Jiang XJ, Lo PC, Yeung SL, Fong WP, Ng DKP. A pH-responsive fluorescence probe and photosensitiser based on a tetraamino silicon (IV) phthalocyanine. Chem Commun 2010;46:3188–90.
[27] Wang A, Zhou L, Fang KL, Zhou L, Lin Y, Zhou JH, et al. Synthesis of novel octacationic and non-ionic 1,2-ethanediamine substituted zinc (II) phthalocyanines and their in vitro anti-cancer activity comparison. Eur J Med Chem 2012;58:12–21.
[28] Zhou L, Zhou JH, Dong C, Ma F, Wei SH, Shen J. Water-soluble hypocrellin A nanoparticles as a photodynamic therapy delivery system. Dye Pigment 2009;82:90–4.
[29] Ferreira J, Menezes PFC, Kurachi C, Sibata C, Allison RR, Bagnato VS. Photostability of different chlorine photosensitizers. Laser Phys Lett 2008;5:156–61.
[30] Liu JY, Lo PC, Jiang XJ, Fong WP, Ng DKP. Synthesis and in vitro photodynamic activities of di-α-substituted zinc (II) phthalocyanine derivatives. Dalton Trans 2009;38:4129–35.
[31] Cui Y, Wu YS, Liu Y, Yang GM, Liu LX, Fu HB, et al. PEGylated nanoparticles of diperylene bisimides with high efficiency of $^1O_2$ generation. Dye Pigment 2013;97:129–33.
[32] Rocha MS, Lucci CM, Longo JP, Galera PD, Simioni AR, Lacava ZG, et al. Aluminum-chloride-phthalocyanine encapsulated in liposomes: activity against naturally occurring dog breast cancer cells. J Biomed Nanotechnol 2012;8:251–6.
[33] Zeballos NCL, Gauna GA, M.Vior CG, Awruch J, Dicelio LE. Interaction of cationic phthalocyanines with DNA. Importance of the structure of the substituents. J Photochem Photobiol B – Biol 2014;136:29–33.
[34] Ongarora BG, Fontenot KR, Hu X, Sehgal I, Satyanarayana-Jois SD, Vicente MGH. Phthalocyanine-peptide conjugates for epidermal growth factor receptor targeting. J Med Chem 2012;55:3725–38.